efficiency of the blocking by the intramolecular proton transfer, and the rate for the metal-catalyzed hydrolysis of dianionic species $1S^{2-}$ stands for that by metal chelation. Comparison of these rates indicates that the blocking of the inhibitory reverse path is achieved much more efficiently by complexation with the trivalent metal ions compared with the intramolecular proton transfer.

Implications to Metalloenzymes. The majority of enzymatic reactions involve covalent intermediates.[25] When the enzymatic process is a substitution reaction, the leaving group of the substrate remains in the vicinity of the reaction site after it is cleaved by the attack of the enzymatic group. The reverse attack of the leaving group at the resultant intermediate, however, should be also very efficient if the leaving group remains in close proximity to the reaction site. Since this retards the overall reaction, the enzyme must separate the leaving group from the reaction site or block the reactivity of the leaving group.

The aspirin derivatives can be viewed as a model for enzyme–substrate complexes. The carboxyl group of an aspirin derivative corresponds to a catalytic group of an enzyme and the acetoxy moiety to the bound substrate. The phenolate group represents the leaving group of the substrate, which should be blocked or separated after cleavage from the ester linkage in order to achieve fast overall rate. The spontaneous reactions of $1S^-$ and $3S^-$ involve intramolecular proton transfer to the phenolate ion from adjacent carboxyl groups. Thus, in the enzymatic processes, proton transfer from an enzymatic group to the leaving group during a substitution process would block the reverse attack by the leaving group. It is noteworthy that carboxyl groups are the most acidic functional groups that are normally available to enzymes.

The metal ion catalysis in the hydrolysis of **1**, especially $1S^{2-}$ indicates that metal complexation of the leaving group can block the inhibitory reverse paths. Furthermore, the blocking by the metal ions is much more efficient than the intramolecular proton transfer in the present study. Thus, metal ions of some metalloenzymes might participate in catalysis by blocking the inhibitory reverse paths through binding at the leaving groups. The concentrations of the metal ions are low in the present study; but, the effective concentration of an active-site metal ion is much greater, and the blocking of the inhibitory reverse paths by the active-site metal ion would be much more efficient than that in the present study.

A variety of metalloenzymes have been discovered in which metal ions participate as Lewis acids.[26] Although extensive studies have been performed on some of the metalloenzymes[1] such as carboxypeptidase A and carbonic anhydrase, the exact roles of the active-site metal ions are unknown.[9,27,28] For many metalloenzymes, various roles have been assigned to the metal ions,[25–28] but the assignment is based mostly on speculation. This is because no decisive physical method is currently available for correct assignment of the catalytic roles of the active-site metal ions. In this regard, the catalytic features disclosed by the studies with small molecules are particularly useful in the study of metalloenzymes. Catalysis by blocking inhibitory reverse paths is a novel catalytic factor for metal ions. This can be utilized not only in the study of inorganic or organic reaction mechanisms but also in the discussion of the mechanistic roles of metal ions in various metalloenzymes.

Acknowledgment. This work was supported by a grant from the Korea Science and Engineering Foundation.

Registry No. 1, 90772-05-7; $FeCl_3$, 7705-08-0; $CuCl_2$, 7447-39-4; $ZnCl_2$, 7646-85-7; 3-carboxysalicylic acid, 606-19-9; dimethyl 3-carboxysalicylate, 36669-06-4; methyl 3-carboxysalicylate, 101670-85-3; aluminum chloride, 7446-70-0.

(25) Spector, L. B. *Covalent Catalysis by Enzymes*; Springer-Verlag: New York, 1982.

(26) Galdes, A.; Hill, H. A. O. *Inorganic Biochemistry*; Hill, H. A. O., Ed.; The Chemical Society: London, 1979; Vol. 1, Chapter 8.

(27) Golding, B. T.; Leigh, G. J. *Inorganic Biochemistry*; Hill, H. A. O., Ed.; The Chemical Society: London, 1979; Vol. 1, Chapter 2.

(28) Pocker, Y.; Sarkanan, S. *Adv. Enzymol.* **1978**, *47*, 149.

Structure of Aridicin A. An Integrated Approach Employing 2D NMR, Energy Minimization, and Distance Constraints

Peter W. Jeffs,* Luciano Mueller, Charles DeBrosse, Sarah L. Heald, and Richard Fisher

Contribution from Smith Kline and French Laboratories, Philadelphia, Pennsylvania 19101.
Received July 5, 1985

Abstract: Elucidation of the structures of aridicin aglycon (**2**) and the parent antibiotic, aridicin A (**8**), are described. Two-dimensional NMR correlation spectroscopy (COSY) and nuclear Overhauser spectroscopy (NOESY) in conjunction with an improved delayed COSY sequence are utilized together with previous chemical data to elucidate the covalent structural framework of the aglycon. Elaboration of the latter to a full three-dimensional structure representing a minimum energy conformation **6** is described by using intramolecular hydrogen–hydrogen distance information derived from the 2D NOE results in conjunction with interactive computer-assisted molecular modeling and force field energy minimization. The full details of positions and stereochemistries of the attachment of mannose and the 2-deoxy-2-[(1-oxodecyl)amino]-D-glucopyranosiduronic acid residue in aridicin A by two-dimensional NMR methods including double quantum experiments are described.

Glycopeptide antibiotics belonging to the vancomycin–ristocetin class[1] have been the subject of much recent interest, owing to the increasing importance of vancomycin for the treatment of methcillin-resistant staphylococcal infections[2] and pseudomembranous colitis[3] plus the development of certain members of these glycopeptides as growth-promotant feed additives for livestock.[4]

The glycopeptide antibiotics exert their biological action by inhibiting bacterial cell wall synthesis by binding to putative cell wall precursors that terminate in L-Lys-D-Ala-D-Ala. The an-

(1) Williams, D. H.; Rajanada, V.; Williamson, M. P.; Bojesen, G. In *Topics in Antibiotic Chemistry*, Part B; Sammes, P., Ed.; Ellis Horwood: Chichester, U.K., 1980; Vol. 5, pp 119–158.

(2) Karchmer, A. W.; Archer, G. L.; Dismukes, W. *Ann. Int. Med.* **1983**, *98*, 477–485.

(3) Cafferkey, M. T.; Hine, R.; Keane, C. T. *J. Antimicrob. Chemother.* **1982**, *9*, 69–74.

(4) Fesik, S. W.; Armitage, I. M.; Ellstad, G. A.; McGahren, W. J. *Mol. Pharmocol.* **1984**, *25*, 275–280.

0002-7863/86/1508-3063$01.50/0

tibiotics are categorized by structures containing a central heptapeptide core incorporating the generalized structure **1**. The

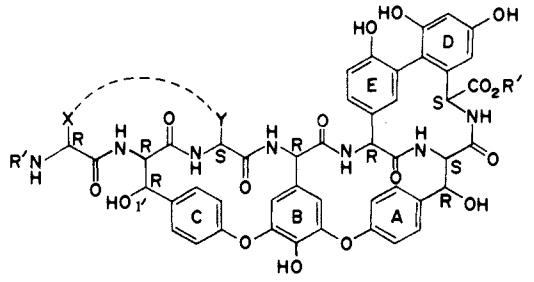

1

amino acid units "X" and "Y" are variable, and although the skeletal framework encompassed within the aromatic amino acid fragments A–E is highly conserved, structural variation also occurs within this region in the number and location of chlorine atoms and the presence or absence of a hydroxyl at C-1′.

The isolation of a new glycopeptide antibiotic complex consisting of the aridicins A–C from *Kibdelosporangium aridum* has been reported recently from this laboratory.[5] In this paper we describe the development of methods using primarily 2D NMR studies in conjunction with computer-assisted molecular modeling to provide a complete three-dimensional structure of aridicin A. The initial goal was to explore the application of modern 2D NMR methods to derive the primary structure of the aglycon that is common to aridicins A–C. Next, we investigated the application of distance constraints obtained from 2D NOESY maps to derive both configurational and conformational features of the aglycon in conjunction with the use of energy calculations and computer-assisted modeling. Finally, we sought NMR procedures to elucidate the stereochemistry of the carbohydrates and the location of the sites of their attachment to the central peptide core in intact aridicin A.

Experimental Section

Materials. Aridicin A (**8**) was isolated and purified from the organism *K. aridum* as previously described.[5] Conversion of aridicin A to the pseudoaglycon **9**, mannosyl aglycon **10**, and the aglycon **2** was accomplished by acid hydrolysis followed by purification by preparative chromatography according to experimental methods and procedures previously described.[6]

Samples for NMR analysis were dried by lyophilization and prolonged pumping and then dissolved in freshly opened deuterated solvents of the highest available purity (99.96% D, Me_2SO-d_6, D_2O, $CDCl_3$). Approximately 10 mg of solid was dissolved in 0.5 mL of solvent for ^1H NMR studies while from 50 to 200 mg was used for the ^{13}C experiments.

NMR Spectroscopy. ^1H NMR. Proton spectra were obtained with either a JEOL GX500 spectrometer operating at 500.1 MHz or a Bruker Instrument WM 360 spectrometer operating at 360.13 MHz. Two-dimensional proton-correlated (COSY) spectra were measured with the WM 360 in the quadrature detection mode with the appropriate phase cycling for N-type peak selection. A spectral window of typically 3000–4000 Hz was employed. The 2D data matrix consisted of 512 2K spectra, which yielded, after zero-filling in F1 and Fourier transformation, a 1-MW square matrix. The data were sine bell apodized and calculated as magnitude spectra. These data were not symmetrized.

The 2D data recorded on the WM 360 were processed with the Aspect 2000A standard software.

All 2D NOE data recorded on the GX500 were transferred to a VAX 11/780 via magnetic tape and processed with software developed by D. Hare.[7] The spectra were calculated in the phase-sensitive mode using the method of Mueller and States et al.[8] The 2D NOE signals were subjected to cosine apodization in both time domains prior to Fourier transformation to avoid truncation effects in the 2D spectra. However, magnitude spectra were obtained from sine bell apodized fid's. Phase-sensitive 2D NOE spectra consisted of 1024 points in each frequency domain, since the t_2 fid's contained 2K points and the t_1 fid's containing 512 points were zero-filled to 1K. Thirty-two scans were accumulated per t_1 fid during which proper phase cycling was applied.[8] At the beginning of the mixing period, a homogeneity spoiling pulse was applied to further suppress unwanted signals[9] (i.e., magnetization transfer due to J coupling). In the 2D NOE spectrum of the aglycon the spectral window was 4812 Hz in both frequency domains, the mixing time was 0.5 s, the relaxation delay was 2.7 s, and the sample temperature was 40 °C. During 2D NOE experiments the samples were not spun in order to reduce t_1 noise. The volume integrals of cross peaks were taken from symmetrized spectra. However, only cross peaks were considered that also appeared in the nonsymmetrized spectra (generally, all spectra were analyzed in the nonsymmetrized form). Volume integrals were computed on square data matrices consisting of 5 × 5 points covering a two-dimensional area of 24 × 24 Hz by using an algorithm developed by D. Hare.[7]

The delayed COSY experiment originally proposed by Bax et al.[10] was slightly modified by selecting a long-interval δ_1 before the mixing pulse (in the order of $1/J_{\text{long range}}$) and only a short-delay δ_2 thereafter. The sum of acquisition time and δ_2 was chosen to be longer than $t_{1\max}$ and δ_1 to ensure proper recording of the full coherence transfer echo.[11] This sequence enabled us to observe magnetization transfer from narrow resonances to broad resonances that would have been lost in a standard experiment. Further, our modification allowed more signal to be recorded in t_2 this way. The spectral widths were set to 4812 Hz, 4K sampling points were recorded in t_2 in the quadrature phase detection mode, and 512 fid's were recorded in t_1, which were zero-filled to 1K. Before the Fourier transformation, a 5° sine bell apodization was applied in t_2, and the t_1 fid's were subjected to a 30° sine bell. The following delays were used in all delayed COSY experiments: δ_1 = 300 ms; δ_2 = 60 ms.

The double quantum experiments were performed with the following pulse sequence proposed by Mueller:[12]

$$P_{90}{}^x\text{–}\tau\text{–}P_{180}{}^y\text{–}\tau\text{–}P_{45}{}^y\text{–}t_1\text{–}P_{135}\text{–acquire}$$

This sequence offers two advantages over the conventional experiment.[13] First, higher order combination transitions in which more than two protons participate are greatly decreased, and second, the 135° read pulse at the end of t_1 permits quadrature phase detection in F_1.[14] This sequence allows the carrier frequency to be placed in the center of the proton spectrum to double the resolution in both frequency domains. Complete suppression of the mirror images of double quantum signals in F_1 would require the read pulse to be near 180°, which would result in a great loss in sensitivity. We found that the mirror images were sufficiently weak to be recognized as such with the read pulse at 135°. The sensitivity is reduced by a factor of 2 in the employed sequence.[12] The preparation interval was 17 ms. The spectral width was 8203.4 Hz in F_1 and 4201.7 Hz in F_2. The sample used in the double quantum experiment was prepared as follows: Aridicin A (12 mg) was dissolved in 0.5 mL of Me_2SO-d_6/H_2O (3:2 volume ratio); the pH was adjusted to 5.7 with 0.1 M trifluoroacetic acid. The 512 t_1 experiments were recorded with 16 scans per t_1 point at 40 °C. The t_2 fid's contained 2048 points. The water peak intensity was reduced by presaturation with low rf power. Sine bell apodization was applied in both time domains. The t_1 fid's again were zero-filled to 1K points. Again, the sample was not spun in order to reduce t_1 noise.

One-dimensional spectra were usually recorded with 8K sampling points in the quadrature phase detection mode in order to optimize digital resolution. J couplings were extracted from spectra whose resolution was enhanced by using Gaussian/exponential windows.

^{13}C NMR. ^{13}C spectra were measured with the Bruker WM360 operating at 90.56 MHz, equipped with either a 10-mm broad-band probe or a 5-mm C/H dual probe. Spectra editing was achieved by using a gated spin-echo experiment with the delay time set at 6.5 ms.[15] Carbon

(5) Sitrin, R. D.; Chan, G.; Dingerdissen, J.; Holl, W.; Hoover, J. R. E.; Valenta, J.; Webb, L.; Snader, K. M. *J. Antibiot.* **1985**, *38*, 561–571.
(6) Jeffs, P. W.; Chan, G.; Sitrin, R.; Holder, N.; Roberts, G. D.; DeBrosse, C. *J. Org. Chem.* **1985**, *50*, 1726–1731.
(7) Hare, D., Infinity Systems Design, Inc., Seattle, WA 98115.
(8) Mueller, L.; Ernst, R. R. *Mol. Phys.* **1978**, *38*, 963–992. States, D. J.; Haberkorn, R. A.; Ruben, D. J. *J. Magn. Reson.* **1984**, *48*, 286–296.
(9) Jeener, J.; Meier, B. H.; Bachmann, P.; Ernst, R. R. *J. Chem. Phys.* **1979**, *71*, 4546–4553.
(10) Bax, A.; Freeman, R. *J. Magn. Reson.* **1981**, *44*, 542–561.
(11) Aue, W. P.; Bartholdi, E.; Ernst, R. R. *J. Chem. Phys.* **1976**, *64*, 2229–2246.
(12) Muller, L. *J. Magn. Reson.* **1984**, *59*, 326–331.
(13) Bax, A.; Freeman, R.; Frenkiel, T. A. *J. Am. Chem. Soc.* **1981**, *103*, 2102–2104.
(14) Marecei, T.; Freeman, R. C. *J. Magn. Reson.* **1983**, *51*, 531–535.
(15) Brown, D. W.; Nakashima, T. T.; Rabenstein, D. L. *J. Magn. Reson.* **1981**, *45*, 302–314.
(16) Dwek, R. A. In *Nuclear Magnetic Resonance in Biochemistry: Application to Enzyme Systems*; Clarendon: Oxford, 1973; p 26, eq 7.1.

spectra for the aglycon were measured at ambient temperature in both Me_2SO and 4:1 (v/v) D_2O/CD_3OD mixtures at pH 8.5 (meter, uncorrected) as solvent. A spectral width of 20 KHz (32K points) proved adequate for the one-dimensional spectra.

Carbon–hydrogen-correlated spectra were measured for **2** by using the

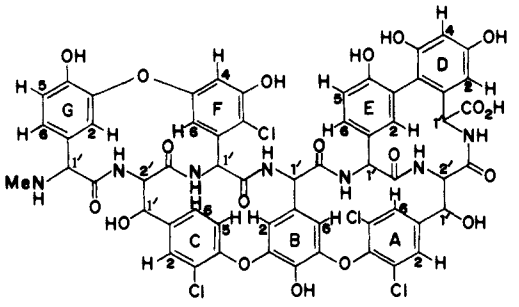

2

sequences in the Bruker software. The sweep width in the carbon (F2) dimension was 16 129 Hz and in the proton (F1) dimension 2800 Hz. Carbon fid's (512), each consisting of 4K data points, were collected with 128 scans per fid. The delay time for transfer of magnetization was 3.7 ms, and the refocusing delay was 1.85 ms. The data were processed by sine bell apodization in both F1 and F2.

Carbon-13 relaxation times were measured for Me_2SO solutions of **2** by using a standard inversion–recovery pulse sequence with 12 randomized τ values. The T_1 measurements were conducted at 40 °C, and the T_1's were processed subsequently by using the nonlinear least-squares three-parameter curve-fitting routine in the Bruker software.

Molecular Modeling. Structures were built in the SK&F molecular modeling system, which consists of an Evans and Sutherland PS330 graphics system linked to a VAX 11785 Digital Equipment Corp. computer. Software employed was a modified version of the SYBYL program (3.0) from Tripos Associates[17] and the MOGLI program from Evans and Sutherland Associates.[18] Model structures were built from a library of structural fragments possessing idealized geometries.

The structures were built in a series of steps: The ADE linear tripeptide was built from individual peptides. The DE macrocyclic ring was closed via the adjustment of internal torsion angles. To the ADE tripeptide (which now included the DE macrocyclic ring) was added the B peptide, and the AB macrocyclic ring closed in a manner similar to that of the DE ring closure. The approach, addition of individual peptides followed by macrocyclic ring closure, was repeated to build the remainder of the peptide. Where more than one set of torsion angles was found that allowed macrocyclic ring closure, the sets that were in best agreement with the NOE data were chosen. In the event that several met the NOE constraints, all acceptable conformations were energy minimized. After each macrocyclic ring-closure step, the newly formed structure was minimized for five to ten steps by using the Tripos simplex minimization program.[19] The simplex minimization method[20] was selected on the basis of its ability to minimize structures with poor initial geometries. The simplex program was not allowed to run to completion, owing to its slow convergence and the intermediate nature of the starting structures. The partially minimized structure was then subjected to 30 cycles of steepest descent minimization with the Tripos MINIM program.[17] The molecular mechanics potential function used by the simplex and MINIM programs included terms related to bond lengths, bond angles, out-of-plane angles, dihedral angles, and nonbonded interactions. The force field parameters and ideal bond lengths and angles are based upon the work of White.[21] At the end of the 20 energy refinement cycles of MINIM, the change in energy was less than 0.1 kcal/mol.

The stereochemistry of the initial structure was systematically modified at the C2′, F1′, B1′, and A2′ chiral centers, with the E1′ stereochemistry being retained as *R* to produce the 16 core structures; stereochemistry at G1′, C1′, A1′, and D1′ centers was initially ignored, and the peptide bonds were set in the trans configuration except for that between amino acid units A and E, which was set in the cis configuration (vide infra). Each modified model was first subjected to 10 cycles of simplex refinement to remove the bad geometries and then to 30 cycles of refinement using the MINIM program.

Each of the models was visually inspected on the SK&F molecular modeling system for abnormal bond lengths and angles, out-of-plane atoms, and unusually close nonbonded atoms. These types of geometrical errors were manually corrected by adjusting torsion angles or, if necessary, by rebuilding to give a new version of which was then subjected to energy refinement.

Scheme I. Interrelationships between the Aridicins and the Products of Acid Hydrolysis

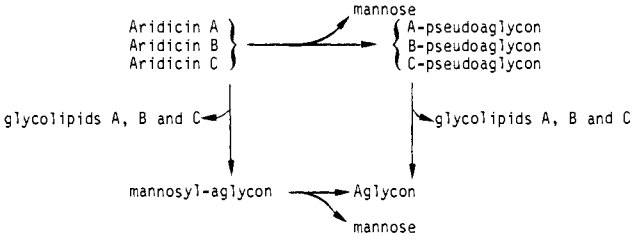

Table I. Classification of Carbon Types Derived from the 90-MHz Edited ^{13}C Spectrum of Aridicin Aglycon Using a Gated Spin-Echo (GASPE) Pulse Sequence

no.	classification
7	carbonyl carbons
25	aromatic carbons containing a substituent
17	aromatic carbons bearing hydrogen
9	methine carbons linked to oxygen or nitrogen
1	carbon of an NMe group

Discussion and Results

At the outset of these studies it was known from previous work[5,6] that the aridicins A–C were based upon a common aglycon. Acid hydrolysis of the individual antibiotics yielded this aglycon together with D-mannose and an *N*-acyl-2-amino-2-deoxyglucuronic acid. Further work has demonstrated that the differences in the aridicins A–C are restricted to structural variations in the nature of the *N*-acyl group in the uronic acid moiety.[6] The interrelationships established from these studies are summarized in Scheme I.

Structure of the Aglycon. Aridicin aglycon is obtained as an amorphous solid from acid hydrolysis of the aridicin complex and subsequent purification of the hydrolysate by reversed-phase preparative HPLC. An accurate mass measurement of the $(M + H)^+$ ion in the fast atom bombardment mass spectrum (FABMS) of the aglycon was in accord with the molecular formula $C_{59}H_{45}N_7O_{19}Cl_4$.

Support for this formula was derived from a comparative study of the ^{13}C spectra of the aglycon in several different solvents by employing both proton noise decoupling and subsequently with a gated spin-echo (GASPE) pulse sequence[15] to provide an edited ^{13}C spectrum at 90 MHz. Both the chemical shift criteria and the editing information, which is summarized in Table I, led to the conclusion that the aglycon was of the ristocetin-type in which seven aromatic rings are present.

Other evidence obtained from experiments undertaken concurrently with the studies reported here has led to the isolation and characterization of actinoidinic acid (**3**) and the bis(amino acid) **4** from the hydrolysis of aridicin aglycon, whereas oxidative degradation of the methylation product of the aglycon yielded the tricarboxylic acid **5**.[22] The information provided by the structures of these degradation products allowed tentative structure **2** to be proposed for aridicin aglycon. With the exception of one detail involving a choice in location of a chlorine atom at position F4 or F6 (see **2**), derivation of this structure can be obtained a priori from a full analysis of the NMR results, but a description of this analysis in a completely rigorous fashion would require an extended and detailed discussion that is not necessary when the structures of the degradation products **3–5** are used. Consequently, the emphasis in this section will deal with the advantages provided by both 2D homonuclear correlation spectroscopy (COSY) and

(17) Tripos Associates, St. Louis, MO 63117.
(18) This is based upon the simplex procedure[19] using modified force fields (Vinter, A. G., unpublished data) based upon those originally described by Bovill and White.[21]
(19) Evans and Sutherland, Salt Lake City, UT 84108.
(20) Nelder, J. A.; Mead, R. *Comput. J.* **1965**, *7*, 308–313.
(21) White, D. N. J.; Bovill, M. J. *J. Mol. Struct.* **1976**, *33*, 273–277.
(22) Sitrin, R.; Chan, G.; Webb, L.; DeBrosse, C.; Jeffs, P. W., submitted for publication in *J. Org. Chem.*

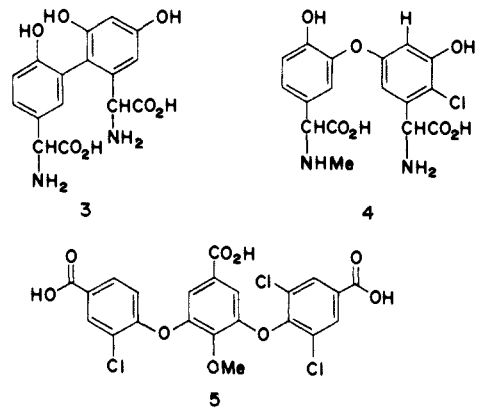

3 4

5

2D nuclear Overhauser (NOESY) experiments in identifying and assigning spin networks and in linking these to provide both extended bond connectivities and through-space relationships in arriving at the primary structure **2** for aridicin aglycon.

Before proceeding with ^{1}H NMR studies of the aglycon, some effort was expended in finding conditions whereby this compound gave well-resolved high-resolution spectra. This was important since other workers have shown that the ^{1}H and ^{13}C spectra of these antibiotics exhibit significant line broadening in their solution spectra, a phenomenon that has been attributed to aggregation effects and/or slow overall rotational tumbling of these molecules (or their molecular aggregates) in Me_2SO_4-d_6.[23] Indeed, measurement of carbon-13 T_1's for the α-carbons at 90.6 and 125 MHz in Me_2SO at 40 °C allowed computation of the rotational correlation time,[16] found to be ca. 3.5×10^{-9} s, suggesting that the aglycons in Me_2SO, at a concentration of ca. 50 mg/mL, are highly aggregated, at least on the time scale of rotational diffusion. We assumed a C_α bond length of 1.11 Å. Isotropic diffusion and lack of rapid segmental motion were inferred from the striking unanimity of T_1's in carbons of similar hybridization and substitution, e.g., the protonated aromatic carbons had $T_1 = 0.20 \pm 0.03$ s at 90.5 MHz. This fact takes on more importance in our subsequent use of proton NOE's to describe relative distances, in which we assume that a single correlation time adequately describes the molecular motion. Although improved ^{1}H NMR spectra are reportedly obtained with compounds in which the carbohydrates have been removed to yield the so-called pseudoglycons (heptapeptide core linked to a single amino sugar) or aglycons, the published spectra of these two classes still show evidence of some line broadening. After some experimentation, conditions were found that gave well-resolved high-resolution 1D ^{1}H spectra of aglycon **2** at 360 or 500 MHz using solutions in either Me_2SO-d_6/$CDCl_3$ (2:1) (solvent A) or Me_2SO-d_6/$CDCl_3$ (1:1) containing 3% CF_3CO_2H (solvent B). The high quality of these spectra is illustrated in Figure 1, which shows the low-field region of the ^{1}H spectrum of **2**. The spectra of **2** obtained under these conditions provide sharp resonance signals for all protons with the exception of the hydroxyl and the terminal amino groups; these latter signals are not observed due to their intermediate exchange rates with residual water in the sample.

The general features of the 1D spectra of **2** reveal (see Table II) an *N*-methyl signal, one 1-H singlet, eight 1-H doublets, and two AB parts of ABX spin patterns in the region δ 4.1–6.1 and a series of well-defined peaks between δ 6.1 and 8.5 representing 15 aromatic protons and six amide NH doublets. The latter were characterized as amide signals by a D_2O exchange experiment. Other significant changes that were noted in the spectrum of the deuterated sample were the simplification of two ABX systems to two AB patterns and the collapse of four (δ 6.08, 5.58, 4.48, 4.13) of the six doublets to singlets. The residual AB(X) patterns were thereby assigned to NH–α-CH–β-CH fragments, and the four doublets undergoing collapse to singlets were attributed to isolated α-CH–NH spins.

(23) Hunt, A. H.; Malloy, R. M.; Occolowitz, J. L.; Marconi, G. G.; Debono, M. *J. Am. Chem. Soc.* **1984**, *106*, 4891–4895.

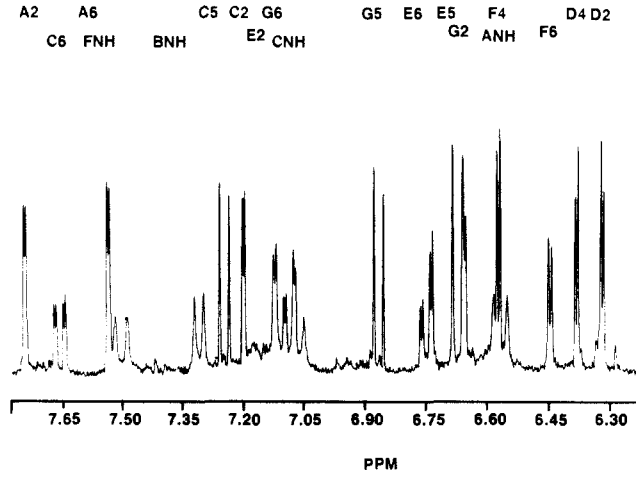

Figure 1. Low-field region of 360-MHz ^{1}H spectrum of aridicin aglycon (**2**) in Me_2SO-d_6/$CDCl_3$ (1:1).

Table II. Proton Chemical Shift Assignments of Aridicin Aglycon (**2**)[a]

peak	solvent A, δ	solvent B, δ	J, Hz	assgnt
1	8.31	8.41	d, 5.8	ENH
2	8.27	8.36	d, 6.0	DNH
3	7.67	7.83	dd, 2.0, 8.5	C6
4	7.07	7.79	d, 8.2	CNH
5	7.76	7.78	d, 1.8	A2
6	7.55	7.57	d, 1.8	A6
7	7.51	7.55	d, 10.5	FNH
8	7.20	7.25	d, 2.0	C2
9	7.25	7.21	d, 8.5	C5
10	7.08	7.21	dd, 8.5, 2.2	G6
11	7.13	7.12	d, 2.2	E2
12	6.88	7.01	d, 8.5	G5
13	7.32	6.95	d, 8.0	BNH
14	6.66	6.83	d, 2.2	G2
15	6.76	6.78	dd, 2.2, 9.0	E6
16	6.67	6.74	d, 9.0	E5
17	6.59	6.65	d, 2.5	F4
18	6.59	6.58	d, 12.0	ANH
19	6.45	6.51	d, 2.5	F6
20	6.39	6.43	d, 2.0	D4
21	6.33	6.36	d, 2.0	D2
22	6.08	6.07	d, 10.5	F1′
23	5.73	5.86	d, 1.8	B6
24	5.58	5.64	d, 8.0	B1′
25	4.26	5.41	s	G1′
26	5.20	5.20	d, 6.6	C1′
27	5.18	5.20	dd, 6.6, 6.5	C2′
28	5.10	5.15	d, 1.1	A1′
29	5.11	5.12	d, 1.8	B2
30	4.48	4.53	d, 6.0	D1′
31	4.40	4.42	d, 5.8	E1′
32	4.13	4.14	dd, 1.1, 12.0	A2′
33	2.38	2.51	s 1	NMe

[a] Chemical shift assignments of aglycon **2**: in solvent A Me_2SO-d_6/$CDCl_3$ (1:1) and 40 °C, pH 3.4; in solvent B Me_2SO-d_6/$CDCl_3$ containing 3% CF_3CO_2H at 56 °C. Coupling constants are reported for solvent B and are derived from a first-order analysis of all spin systems with the exception of the ABX pattern from C1′, C2′, and CNH, which was analyzed in solvent B (and several other solvents) by the spin simulation program PANIC (Bruker software).

Of the remaining three signals in the δ 4.1–6.1 region that are unaffected by deuterium exchange, the chemical shift of the singlet shows a marked sensitivity to pH; it occurs at δ 4.26 in solvent A and δ 5.41 in solvent B. Assignment of this signal to an α-CH– at the N terminus of the peptide chain is consistent with the prediction that the change in charge density on the adjacent protonated nitrogen strongly influences the chemical shift of this α-CH group.

The other two doublets (δ 5.12 and 5.86, J = 1.8 Hz), which are mutually coupled, were assigned to aromatic protons despite the unusually highly shielded value of their chemical shifts. This

Chart I. Structural Fragments of Isolated Proton Spin Networks Present in Aridicin Aglycon[a]

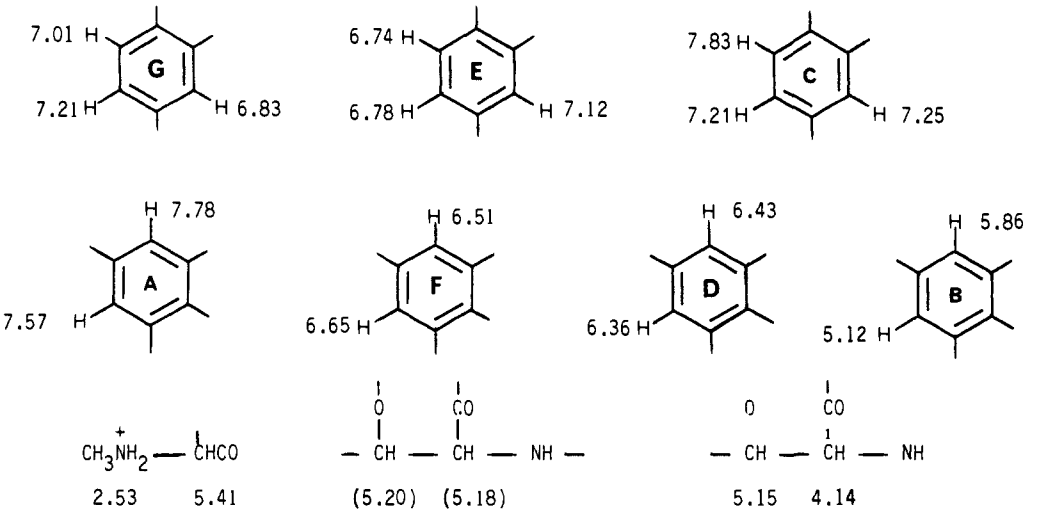

[a] All shifts are reported for solvent B except those in parentheses, which are in solvent A. The shifts of four AB spin patterns originating from four α-CH–NH units are omitted.

assignment was indicated initially by comparisons with other glycopeptide antibiotics, including vancomycin (δ 5.63 and 5.18);[24] however, independent confirmation was clearly and most conclusively provided by the 2D heteronuclear shift ^{13}C–^{1}H spectrum of **2** that showed that the proton signals at δ 5.86 and 5.12 are linked to carbons with chemical shifts of 108.7 and 103.8 ppm, respectively (see Table III). The carbon chemical shifts derived from the 2D ^{13}C–^{1}H shift correlation map also provided confirmatory evidence for the α-CH proton assignments and, furthermore, indicated the two β-CH signals with chemical shifts at 71.2 and 70.2 ppm represent carbons bearing an oxygen function.

Two-dimensional ^{1}H homonuclear correlation spectroscopy (COSY) was used to confirm the proton assignments of the peptide backbone and characterize the aromatic ring hydrogens. In addition to the high-field m-coupled doublets at δ 5.12 and 5.86 mentioned earlier, six additional aromatic spin systems representing two m-coupled pairs and four AMX patterns characteristic of 1,3,4-trisubstituted rings were readily apparent from the proton–proton *J* connectivities revealed by the appropriate cross peaks in the COSY spectrum (Figure 2a). Furthermore, the relationships of the four α-CH–NH and two β-CH–α-CH–NH spin networks were also characterized from the COSY spectra (Figure 2b). With the exception of the four α-CH–NH units, the substructural units, which were identified from the ^{1}H COSY spectra, are shown in Chart I.

For all of the spin systems characterized, translation of this information to structural details was approached by using two spectroscopic methods. One of these was a modified 2D COSY experiment (see Experimental Section for details of the pulse sequence used) that results in spectra with considerably magnified cross peaks induced by long-range *J* couplings.[10] This procedure offers the potential of determining extended bond connectivities across isolated spin systems. The second method involved two-dimensional nuclear Overhauser enhancement (NOESY) spectroscopy, which allows short, through-space connectivities to be established.

To facilitate discussion of the synthesis of the spectral results in deriving structural information, we have used the nomenclature system employed previously by Hunt and co-workers[26] for this series of antibiotics. The seven aromatic rings are lettered A–G, and the peptide backbone atoms associated with individual aromatic rings are identified by the same letter code and differentiated from the ring atoms by a primed numerical descriptor.

Table III. Proton–Carbon Correlated Chemical Shifts of Aglycon **2** in Me_2SO-d_6 Obtained from 2D ^{1}H–^{13}C Heteronuclear COSY Spectrum[a]

α	chem shifts, δ H′	chem shifts, δ ^{13}C	assgnt
1	2.38	33.7	CH_3-NH
2	4.35	54.0	E1′
3	4.41	57.2	D1′
4	4.45	65.7	G1′
5	5.06	103.8	B2
6	5.09	71.2	A1′
7	5.12	60.2	C2′
8	5.12	70.2	C1′
9	5.65	55.0	B1′
10	5.67	108.7	B6
11	6.02	54.0	F1′
12	6.30	106.5	D2
13	6.36	102.5	D4
14	6.52	105.5	F6
15	6.58	106.5	F4
16	6.65	117.4	E6, E5, G2
17	6.67	126.0	
18	6.90	118.2	G5
19	7.06	135.7	E2
20	7.11	126.0	G6
21	7.20	128.6	C2
22	7.28	125.0	C5
23	7.53	128.0	A2
24	7.75	125.0	A6
25	7.75	127.4	C6

[a] A2′ is not found.

The 2D delayed COSY spectrum of **2** obtained in solvent B provided a rich source of cross peaks originating from both normal and long-range couplings (see Figure 2). Extension of bond connectivities from each of the seven aromatic rings into the backbone was revealed by the occurrence of cross peaks between the benzylic protons and ortho and/or para protons in the attached rings. Although observation of the long-range coupling of ortho ring protons to the benzylic position was not unexpected, it was surprising and gratifying that these couplings were observed in all seven rings. Since the magnitude of this coupling is known to have a strong orientational dependency,[27] it seemed unlikely that all seven rings would be optimized for the observation of this

(24) Williams, D. H.; Kalman, J. R. *J. Am. Chem. Soc.* **1977**, *99*, 2768–2778.

(25) Steffens, J. C.; Roark, J. L.; Lynn, D. G.; Riopel, J. L. *J. Am. Chem. Soc.* **1983**, *105*, 1669–1671.

(26) Hunt, A. H. *J. Am. Chem. Soc.* **1983**, *105*, 4463–4468. The priority of numbering of the various rings changes with changing substitution patterns, and therefore, cognizance of this should be taken into account when making comparisons of chemical shifts, etc., between the various members of this class.

(27) Barfield, M.; Fallick, C. J.; Hata, K.; Sterhell, S.; Westerman, R. W. *J. Am. Chem. Soc.* **1983**, *105*, 2178–2186. Sternhell, S. *Q. Rev. Chem. Soc.* **1969**, *23*, 236–270.

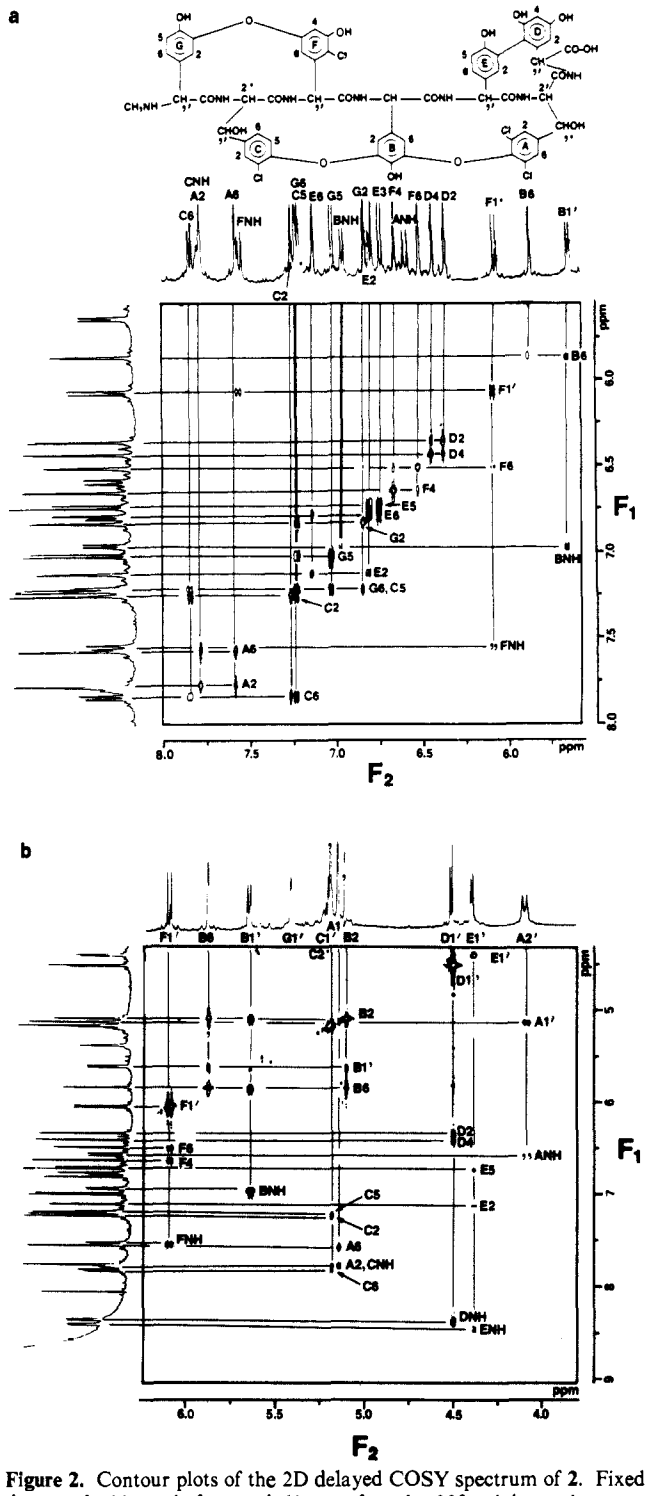

Figure 2. Contour plots of the 2D delayed COSY spectrum of 2. Fixed delays of 300 ms before and 60 ms after the 90° mixing pulse were inserted. Spectrum was recorded at 56 °C. A total of 502 t_1 fid's was collected each of which having a length of 0.42 s. The spectra show (a) ^1H–^1H correlations of aromatic spin networks and (b) ^1H–^1H correlations involving NH and backbone α- and β-CH spin systems.

effect. Equally surprising was the recognition of six-bond long-range coupling between the para hydrogens on rings D and F with the respective benzylic α-CH protons D1′ and F1′. Although precedent exists for such long-range coupling, very few examples have been reported.[28]

Further significant observations from the delayed COSY experiments involved two cases of magnetization transfer between sets of protons on different residues. The specific assignments

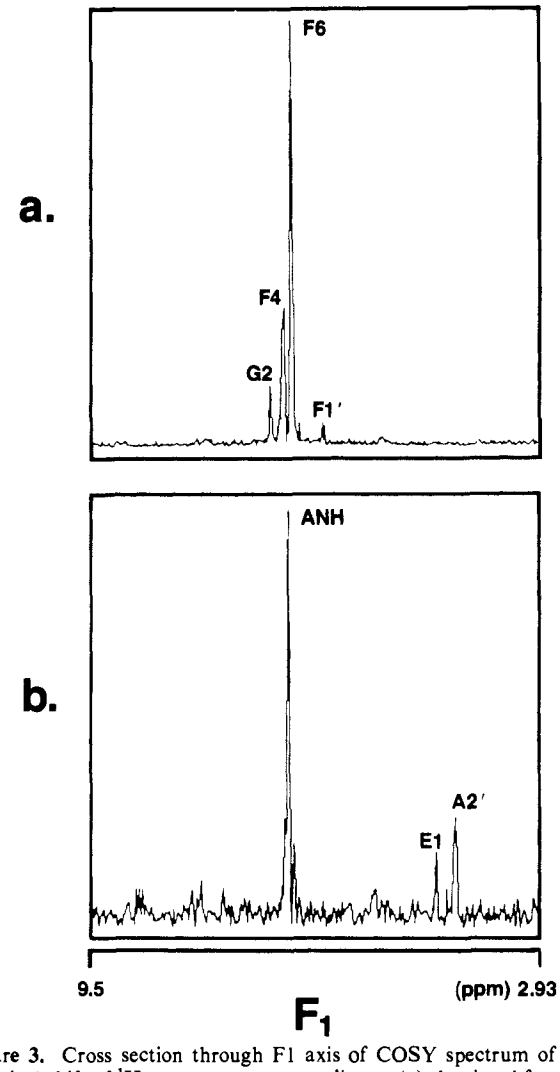

Figure 3. Cross section through F1 axis of COSY spectrum of 2 at chemical shift of ^1H resonance corresponding to (a) the signal from the F6 hydrogen showing J connectivities to G1′, F4, and G2 hydrogens and (b) the signal from ANH showing J connectivities to E1′ and A2′ hydrogens.

of the protons involved was ultimately dependent on interpretation of the NOESY data reported below that allowed the conclusion to be made that they involved the interresidue coupling between hydrogens F6 and G2 and hydrogens ANH and E1′, respectively. These highly intriguing results are clearly revealed in Figure 3 in which cross sections through the COSY contour plots at the chemical shifts of the F6 and ANH protons in the F1 frequency axis are displayed. It is important to note that it would have been most unlikely, if not impossible, to have detected any of these long-range ^1H couplings by conventional 1D methods, including difference spectroscopy.

While the foregoing data provided useful information that allowed the association of aromatic ring hydrogen spin with specific backbone spin patterns, it did not provide any information on the *sequence* of the peptide units in the backbone. The details related to this question were elucidated from determining the spatial proximity of neighboring protons through observation of nuclear Overhauser effects (NOE).

In order to assess the spatial relationship of the spin systems described above, the NOE's in aridicin aglycon were examined by two-dimensional cross-relaxation spectroscopy. This 2D NOE (NOESY) experiment has several advantages over conventional 1D experiments such as NOE difference spectroscopy, which has been used previously to good effect by Williamson[29] and Hunt[30]

(28) Rottendorf, H.; Sternhell, S. *Tetrahedron Lett.* **1963**, 1289–1295. Rottendorf, H.; Sternhell, S. *Aust. J. Chem.* **1964**, *17*, 1315–1328.

(29) Williamson, M. P.; Williams, D. H. *J. Am. Chem. Soc.* **1981**, *103*, 6580–6585.

Table IV. Nuclear Overhauser Enhancement Results for Compound **2** and Comparisons of ^1H–^1H Distance Data with the Model **6**

proton	cross peak (intens)[a]	^1H–^1H dist[b] from model **6**, Å	proton	cross peak (intens)[a]	^1H–^1H dist[b] from model **6**, Å
A1′	A2 (2)	2.36	C6	FNH (3)	3.60
	A2′ (2)	2.55	CNH	G1′ (3)	2.19
	DNH (3)	3.42		C1′ (3) or C2′ (3)	3.70 or 2.94
A2′	E1′ (1)	1.79		FNH (2)	2.48
	DNH (2)	1.98	D1′	DNH (2)	2.93
	E2 (2)	2.54		E2 (3)	(4.24)
	A2 (3)	2.97	DNH	E2 (2)	1.82
A2	E1′ (3)	3.90		E1′ (2)	3.07
	DNH (3)	3.90	E1′	E2 (1)	2.36
A6	ANH (3)	2.73		ENH (3)	2.85
B1′	ENH (1)	2.09	E6[c]	ENH (3)	3.04
	B6 (3)	2.93	F1′	FNH (3)	2.94
	B2 (3)	3.31		F6 (3)	3.73
B2	BNH (3)	2.97	F6	FNH (2)	2.54
B6	E1′ (3)	2.80		G2 (3)	2.59
	ENH (3)	3.10	FNH	C1′ (3) or C2′ (3)	3.63 or 3.83
BNH	FNH (3)	2.85		G2 (3)	(4.08)
	F6 (3)	1.90	G1′	G6 (3)	2.45
C1′	C2 (1)	2.38		NMe (3)	2.77
C2′	FNH (3)	3.63	G5	G6 (2)	2.48
C5	C6 (2)	2.48	G6	NMe (3)	(4.17)

[a] Volume integrals were computed from symmetrized spectra on square data matrices (5 × 5 points; 24 × 24 Hz) by using an algorithm development by Hare.[7] The spectra were obtained in solvent B at 40 °C. [b] Distances in parentheses are considered too great to account for the observed NOE results. The hydrogens involved may be at positions in the energy-minimized structure that occupy regions where some conformational flexibility exists so as to allow access to other low-energy conformational states in which these distances are within 3.50 Å. This explanation is preferred over one in which spin diffusions are involved since NOE's are observed between these particular hydrogens at mixing times of 0.2 s. [c] A cross peak is present between the E6 and E5 hydrogens, but because of the proximity of the peaks to the diagonal it was not possible to measure its volume integral with confidence.

and their respective co-workers for studies in this series of antibiotics. The principal advantage of the NOESY experiment is that it overcomes the need for high selectivity in preirradiation of individual resonances in crowded regions of the spectrum, and consequently the range of NOE's observed in complex molecules is usually much more extensive than those obtained from 1D experiments.

Preliminary NOE difference measurements at 360 MHz on **2** in both solvent systems provided no enhancements at 40 °C. However, substantial (10–30%) negative NOE's are observed on cooling the samples to 20 °C, presumably due to an increase in the rotational correlation time τ_c such that $\tau_c\omega_H^2 > 1$, a condition that leads to negative NOE's.[31] This condition is even more favorable at 500 MHz, illustrating the advantage of using the highest possible field strengths in the NOE studies of molecules of this size.

Two experiments with mixing times of 0.2 and 0.5 s were evaluated on the basis of a preliminary examination of NOE buildup rates.[33] The latter value to a first approximation approaches a maximum t_m interval before spin diffusion is manifested. Under the latter conditions a total of *42* cross peaks are observed, which can be confidently attributed to NOE's. The intensity of these cross peaks vary, and although correlations between intensity and proton–proton distances are usually only semiquantitative,[34] we have classified them (Table IV) relative to the intensities as measured by the volume integrals of the NOE's observed for the ortho protons, e.g., C5 and C6, which are at a fixed distance (d_0) of 2.48 Å. Cross peaks are classified into three categories: (1) Those that are more intense than those observed for the ortho protons are listed in class 1 ($d < 2.47$ Å). (2) Peaks of approximately the same intensity are placed in class 2 ($d \sim 2.48$ Å). (3) Those peaks that have smaller integrals than the reference peaks are placed in category class 3 ($d > 2.49$ Å).

The first level of information extracted from the NOESY data established the relative positions of the rings along the amide backbone. The superficial similarity of the various aromatic proton spin patterns made it necessary to begin the analysis by using the *N*-methyl signal as the unique feature of the ^1H spectrum. First, the individual protons related by the NOE to the *N*-methyl were identified. The *N*-methyl signal shows NOE's to aromatic signals at δ 7.21 and 6.83 and the α-CH singlet at δ 5.41. The latter signals had been previously related by the COSY results, with an aromatic ring exhibiting an ABX spin network and its associated benzylic α-CH. This allows the placement of this aromatic ring, now designated as ring G, and its associated backbone protons at the *N*-methyl terminus. By continuation of this process, a strong NOE between G2 and the m-coupled doublet at δ 6.65 allowed the positioning of a second aromatic spin network (ring F) in a contiguous relationship to ring G. The through-space connectivity of G2 and F6 was complemented by the *J* connectivity between these two protons revealed by six-bond long-range coupling indicated in the delayed COSY experiment. Through extension of this process of building up successive "layers" of signals related by proximity, the position of the ABX aromatic spin system designated as ring C was ascertained by the connectivities linking the G1′ and FNH signals with the signal at δ 7.79 (CNH) and the FNH with the signal at δ 7.78 (C6). By continuation of this process, which is most easily visualized through reference to Chart II, key through-space connectivities were identified that allowed the sequence of the remaining rings A, B, D, and E to be assembled as shown.

A number of the assignments of the aromatic ring protons derived from the NOE data are supported by the selective chemical shift changes that are observed when the spectra of the aglycon obtained in solvents A and B are compared. In addition to the large downfield shift of the G1′ proton signal discussed previously, the carbon-bound proton signals C6, G2, G5, and G6 undergo small but significant downfield shifts in solvent B, which contains 3% of CF_3CO_2H. These protons, with the possible exception of C6, are all in close proximity to the cationic methylammonium ion site of the aglycon, which would exist under acidic conditions. This information when considered in conjunction with the extended

(30) Hunt, A. H.; Debono, M.; Merkel, K. E.; Barnhart, M. *J. Org. Chem.* **1984**, *49*, 635–640. Hunt, A. H.; Elzey, T. K.; Merkel, K. E.; Debono, M. *Ibid.* **1984**, *49*, 641–645.

(31) Noggle, J. H.; Schirmer, R. E. *The Nuclear Overhauser Effect, Chemical Applications*; Academic: New York, 1971.

(32) Dill, K.; Allerhand, A. *J. Am. Chem. Soc.* **1979**, *101*, 4376–4378.

(33) Bothner-By, A. A.; Noggle, J. H. *J. Am. Chem. Soc.* **1979**, *101*, 5152–5155. Kumar, A.; Wagner, G.; Ernst, R. R.; Wuthrich, K. *Ibid.* **1981**, *103*, 3654–3658.

(34) Recent work has described the use of nuclear Overhauser enhancements to obtain quantitative distance information. See: Burch, M.; Noggle, J. H.; Gierasch, L. M. *J. Am. Chem. Soc.* **1985**, *107*, 1400–1607. Keepers, J. W.; James, T. L. *J. Magn. Reson.* **1984**, *57*, 404–426.

Chart II. Through-Space Connectivity Maps Derived from ^1H-^1H Nuclear Overhauser Effects Obtained from 2D NOESY Spectra of Aridicin Aglycon[a]

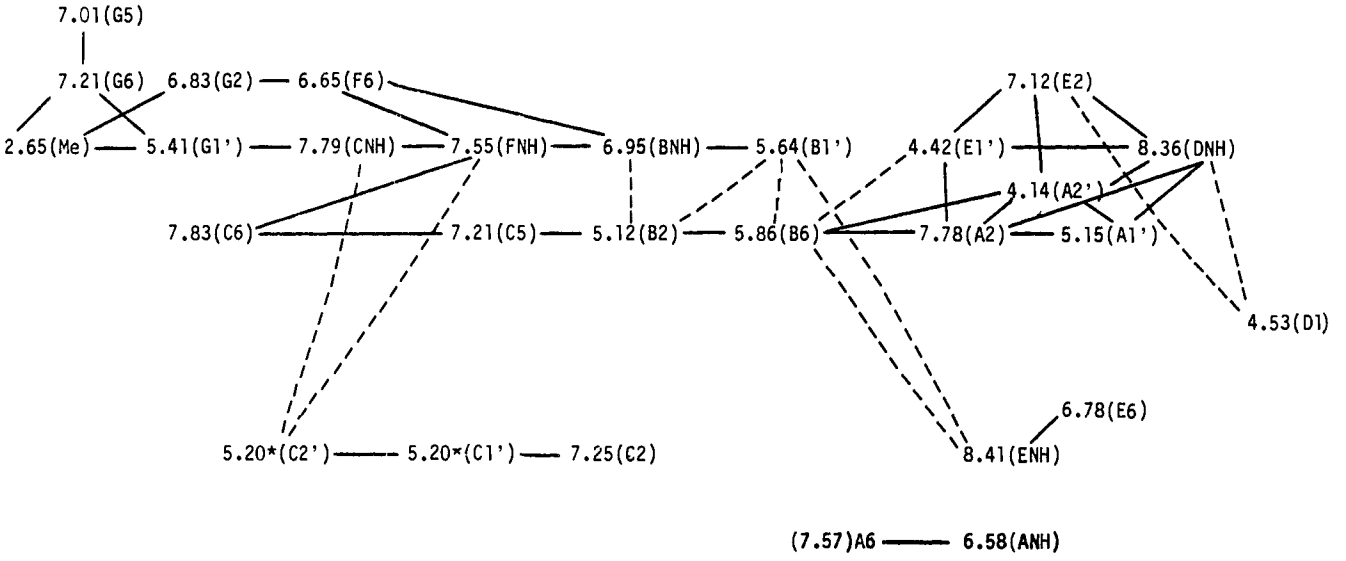

[a] Solid lines (—) indicate NOE's ocurring in the direction of the long axis of the molecule. Dotted lines (---) indicate NOE's occurring in the direction of the short axis, i.e., front face to back face. (*) C1′ and C2′ NOE's were established in solvent system A in which they have different chemical shifts. All other NOE's reported were obtained in me_2SO-d_6/$CDCl_3$ (1:1) containing 3% CF_3CO_2D.

connectivities provided by the delayed COSY experiment provides essentially all of the structural details embodied in structure **2** for the aglycon.

If, at this stage, consideration is given to the structures of the three degradation products **3–5** established previously,[22] structure **2** becomes the only plausible candidate for aridicin aglycon.

Stereochemistry of Aridicin Aglycon. Given the specificity for binding D-Ala-D-Ala residues exhibited by all members of this class of glycopeptides, it is reasonable to expect that the stereochemical features of the peptide backbone of the central peptide core should be conserved in all antibiotics of this class. Consistent with this expectation, strong correlations have been found between the NMR chemical shifts, coupling constants, and NOE data of various members and those of vancomycin.[23,30] This is significant since the stereochemistry of vancomycin has been established from an X-ray structure determination of CDP-I, a rearrangement product of vancomycin.[35]

While it would have been possible to employ the same type of correlations in deriving the stereochemistry of the aridicin aglycon, the extensive NMR data provided by the 2D ^1H NMR experiments suggest that it might be possible to derive the 3D structure of the aglycon a priori by using distance constraints derived from the NOESY data in conjunction with energy minimization and molecular modeling.

Previous application of the distance constraint approach using experimental data derived from NOE measurements has been directed at providing spatial information on protein structures in which the primary stereochemical configurational details are known from the amino acid sequence.[36] However, since the conformation space occupied by a particular structure is dependent on both configurational and conformational characteristics, the use of distance constraint data to elucidate primary structural details of the configuration features of complex structures was an interesting challenge.

At the outset this presented a seemingly formidable task since the number of stereoisomers possible for the aglycon is very large (nine chiral carbons and six peptide bonds = two[15] structures). To reduce this to a manageable number of structures that might reasonably need to be considered, several strategies were developed. Of the nine chiral centers present in **2**, seven are derived from amino acid α-CH groups. If one views the structure of the aglycon as containing four macrocyclic rings, five of the chiral centers represented by C2′, F1′, B1′, E1′, and A2′ are common to two macrocycles whereas the remaining four, i.e., G1′, C1′, A1′, and D1′, are part of a single macrocyclic ring. Consequently, the chirality of the latter four atoms can be inverted by exchanging the two ligands external to the macro ring without effecting the parent macrocycle. The E1′ center was arbitrarily assigned as having the *R* configuration since both the NMR methods and calculations are necessarily restricted to elucidation of relative and not absolute stereochemistry.

Since the ^{13}C NMR of the aglycon shows only a single resonance for the carbons of the peptide backbone, each of the peptide bonds may be assumed to exist predominantly in a single configuration. In addition, it was clear from the observation of a strong NOE between the α-CH protons E1′ and A2′ that these hydrogens must be <3.5 Å apart, which, as noted previously for vancomycin, implies that the peptide bond between the A and E residues must be cis.[29] In view of the probable comparative rigidity suggested by the carbocyclic framework of a structure such as **2** (without stereochemical implications), a very similar range of effective correlation times (τ_c) for all of the α-CH protons may be assumed. This is borne out by the ^{13}C t_1 values and the insensitivity of any $^3J_{NHCH}$ values to temperature over a range of 80 °C. Therefore, the failure to observe NOE's between the α-CH pairs of any other residue in the backbone suggests that the remaining five peptide bonds are trans. Parenthetically, the observation of the unusual interresidue long-range coupling of the E1′ hydrogen to the ANH proton is undoubtedly a reflection of the cis geometry of the peptide bond through which the coupling occurs. Interestingly, this appears to be the first experimental confirmation of an earlier theoretical study in which it was predicted that a cis peptide should show a significant enhancement of long-range interresidue coupling between the NH and α-CH of adjacent residues for θ angles in the range from −40° to −80°, whereas no such coupling is predicted to occur in trans peptides.[37]

To initiate the modeling studies, structures corresponding to the 16 stereoisomers representing the possible stereochemical combinations of the chiral centers C2′, F1′, B1′, and A2′ were generated in the SK&F molecular modeling system. As previously indicated, the E1′ center was held as a reference chiral center in the *R* configuration and the peptide bond between A and E rings was established in the cis configuration while the remaining peptide bonds were constructed with trans stereochemistry. The chirality

(35) Sheldrick, G. M.; Jones, P. G.; Kennard, O.; Williams, D. H.; Smith, G. A. *Nature (London)* **1978**, *271*, 223–225.

(36) Wutrich, K.; Wider, G.; Wagner, G.; Braun, W. *J. Mol. Biol.* **1982**, *155*, 311–319.

(37) Ostlund, N. S.; Pruniski, M. J. *J. Magn. Reson.* **1974**, *15*, 549–563.

at the other chiral centers A1′, D1′, C1′, and G1′, which are "outside" the central core, were eliminated by substituting hydrogen for the non-hydrogen ligand in each of these 16 structures.

The stereochemistry of the initial structure was modified at four of the five internal chiral centers (E1′ was held in the *R* form) and subjected to energy minimization to produce the 16 core structures. The resultant structures were visually inspected on the graphics system and structural differences noted. Two conformations with a difference sense of twist of the F and G phenyl rings were frequently observed and had an energy difference of ~5 kcal. The structure with the lower energy places the F6 hydrogen in toward the front face and the G2 hydrogen directed out to the rear convex face (cf. **6a**). This conformation is in agreement with the NOE results (NOE from F6 to FNH) and was retained in all subsequent models evaluated.

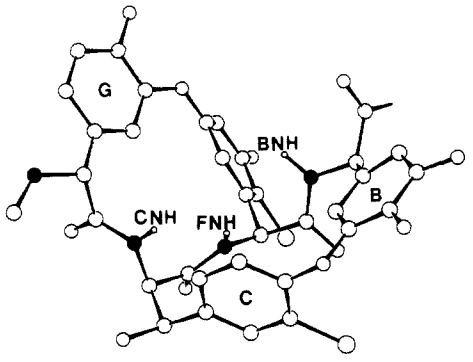

6a

In a preliminary evaluation of the 16 stereochemically different "core" structures, the internuclear hydrogen–hydrogen distances corresponding to the 13[38] strongest NOE's were tabulated (Table V). Of the 16 core structures only two showed all 13 computed internuclear hydrogen distances within an arbitary (and generous) distance limit set at 3.50 Å. The two isomers, structures VII and VIII, have backbone configurations of *S*-F1′, *R*-C2′, *R*-B1′, *R**-E1′, *S*-A2′, and *S*-F1′, *S*-C2′, *R*-B1′, *R**-E1′, *S*-A2′, respectively.

The remaining 14 structures were provisionally rejected since the conformations determined for these structures did not conform to the NOE distance constraints. Furthermore, attempts to induce conformational changes on these structures to fit the distance constraints were unsuccessful.

To ensure that all possible macrocyclic ring conformations were considered, the TRIPOS conformational search program was used to vary the torsion angles so that all possible angle combinations would be evaluated. This procedure requires that a bond within the macrocyclic ring be removed and dummy atoms be placed at the positions of the previously bonded atom. The torsion angles were varied from 0 to 360° for freely rotating bonds, from −20° to +20° for cis peptide bonds, and from 160° to 200° for trans peptide bonds. Structures were accepted if there were no bad interatomic interactions (less than 90% of the sum of the van der Waals radii) and the ring was "closed" (the dummy atoms were within 0.5 or 0.75 Å of their bonding positions).

A comparison of the short intramolecular ^{1}H–^{1}H distances calculated for the two isomers VII (*SRRRS*) and VIII (*SSRRS*) with the experimentally determined NOE's for **2** can be interpreted to provide a compelling argument in favor of the isomer with the *SRRRS* core configuration. In the latter structure an NOE is observed for *all* ^{1}H–^{1}H distances that are calculated to be <3.50 Å whereas the *absence* of strong NOE's between C2′ and CNH and between C2′ and FNH, which are computed at ^{1}H–^{1}H distances of 2.77 and 1.95 Å, respectively, in the *SSRRS* isomer constitutes good reason to reject this structure.

(38) Six strong NOE's that involve hydrogens at A1′, C1′, D1′, and G1′ are not included in this preliminary evaluation since interactions at these sites are at chiral centers that are common to a single macrocyclic ring and are therefore outside the core with chiral centers common to two macrocycles.

Table V. Selected ^{1}H–^{1}H Distance Data for 16 Diastereoisomers Representing the Central Heptapeptide Core of **2**

	I	II	III	IV	V	VI	VII	VIII	IX	X	XI	XII	XIII	XIV	XV	XI
							Configuration									
F1′	*R*	*R*	*R*	*R*	*S*	*S*	*S*	*S*	*R*	*R*	*R*	*R*	*S*	*S*	*S*	*S*
C2′	*R*	*S*	*R*	*S*	*R*	*S*	*R*	*S*	*R*	*S*	*R*	*S*	*R*	*S*	*R*	*S*
B1′	*R*	*R*	*R*	*R*	*R*	*R*	*R*	*R*	*S*	*S*	*S*	*S*	*S*	*S*	*S*	*S*
E1′	*R*	*R*	*R*	*R*	*R*	*R*	*R*	*R*	*R*	*R*	*R*	*R*	*R*	*R*	*R*	*R*
A2′	*R*	*R*	*S*	*S*	*R*	*R*	*S*	*S*	*R*	*R*	*S*	*S*	*R*	*R*	*S*	*S*
							Computed Distance, Å									
A2′–E1′	4.08	4.10	1.83	1.86	4.11	4.10	1.83	1.83	4.12	4.11	1.83	1.86	4.09	4.10	1.81	1.83
B1′–ENH	2.47	2.40	2.44	2.42	2.47	2.40	2.39	2.42	3.40	3.42	3.39	3.45	3.37	3.34	3.39	3.39
E1′–E2	2.81	3.06	3.23	3.22	3.17	3.12	3.14	3.15	2.88	3.15	3.15	3.19	3.12	3.13	3.13	3.14
FNH–F6	3.91	4.23	3.97	4.24	2.64	2.70	2.69	3.09	3.88	4.13	4.08	4.13	2.70	2.70	2.64	2.59
C5–C6	2.48	2.49	2.48	2.49	2.49	2.48	2.48	2.49	2.48	2.50	2.47	2.49	2.48	2.48	2.48	2.48
E6–E5	2.47	2.47	2.48	2.48	2.48	2.48	2.48	2.48	2.47	2.48	2.47	2.47	2.48	2.48	2.48	2.47
G5–G6	2.48	2.47	2.48	2.48	2.48	2.47	2.48	2.47	2.48	2.48	2.47	2.48	2.48	2.47	2.48	2.47
A2′–DNH	3.63	3.59	2.04	2.06	3.57	3.60	2.11	2.11	3.56	3.55	2.07	2.07	3.62	3.57	2.08	2.09
A2′–E2	3.12	3.31	2.80	2.83	3.32	3.23	2.71	2.71	3.26	3.39	2.78	2.78	3.19	3.32	2.74	2.74
BNH–B2	3.26	3.21	3.16	3.14	2.99	3.15	3.15	3.16	3.49	3.59	3.63	3.47	3.90	3.89	3.90	3.93
DNH–E2	2.69	3.02	3.16	3.13	3.10	3.16	2.88	2.87	2.79	3.02	3.05	3.08	3.24	3.08	2.95	2.94
DNH–E1′	3.44	3.19	3.39	3.38	3.06	3.25	3.25	3.35	3.34	3.09	3.35	3.39	3.29	3.10	3.31	3.33
F6–G2	2.00	1.94	2.09	1.99	1.98	1.95	1.99	1.78	2.06	1.97	2.11	1.96	2.00	1.93	1.95	1.92

Of the remaining four chiral centers at A1′, C1′, D1′, and G1′, the assignment of the *S* configuration at D1′ was indicated from the absence of any strong NOE's to the proton at this center. This conclusion was evident from a comparison of the environment of the D1′ hydrogen on inspection of models of the *R* and *S* isomers that showed that the *R* isomer has several proximal hydrogens (A2′, DNH, and E2) to the D1′ hydrogen whereas the *S* isomer with the D1′ hydrogen appearing on the back face has no neighboring hydrogens on this face that are in close range (<3.5 Å). This assignment was confirmed during the course of the NMR study by the isolation of the optically active actinoidinic acid **3** of established absolute configuration from controlled acid hydrolysis of **2**.[22] While this leaves only the three centers, A1′, C1′, and G1′, to assign, there are several topological features of structure **2** that require consideration.

The arguments developed for the elucidation of these remaining stereochemical features are derived from interlocking experimental evidence in which the configurational and conformational features have many interdependent relationships. It is clear from previous studies on vancomycin that the energy barrier to rotation of rings A and C around the respective A1–A4 and C1–C4 ring axes is sufficiently high that discreet, noninterconvertable atropisomers may exist.[39] A similar situation clearly exists in aridicin aglycon as evidenced by the NOE data. This is manifested by the hydrogen at C6 exhibiting an NOE to the FNH hydrogen that is situated on the concave or binding face, whereas the hydrogen at C2 has a very strong NOE to the C1′ hydrogen that is necessarily located on the convex face and therefore permits the assignment of stereochemistry at C1′ as *R*. A further implication of the above result is that by defining the spatial dispositions of the hydrogens at C2 and C6 as discussed, the chlorine on ring C can be positioned on the edge of the ring that is pointed in the direction of the outer face of the molecule. This particular orientation corresponds to that previously established for the chlorine at the equivalent site in vancomycin.[28-30]

Similar arguments concerning conformational restriction may be made for ring A where the A2 and A6 hydrogens show not only discreet chemical shifts but also exhibit NOE's to hydrogens that are situated on opposite faces. This is exemplified by NOE's from A2 to hydrogens E1′ A1′, and A2′, which are located on the interior of the binding face, whereas A6 shows a single NOE to the ANH. This allows the assignment of the stereochemistry at the benzylic A1′ center as the *S* configuration.

The G1′ center was readily assigned the *R* configuration on the basis of the NOESY spectra of **2**. In this instance it was necessary to interpret information obtained from spectra run in both solvent A and solvent B to overcome certain ambiguities that originated from overlap of resonances of interest. In solvent A a network of NOE's exists that establishes the proximity of hydrogens at G1′, CNH, and C6, whereas in solvent B cross peaks were observed in a NOESY spectrum from CNH to both FNH and G1′. Both sets of results can only be accommodated by assignment of the *R* configuration to G1′. This result is in accord with the recent reassignment of the stereochemistry of ristocetin at this center, which was based upon convincing results from chemical studies by Harris and co-workers.[41]

The one potential difficulty resulting from this configurational assignment at G1′ in aridicin aglycon and ristocetin is the need to account for the changes in the chemical shifts of the CNH (0.72 ppm) and C6 (0.16 ppm) protons that occur on protonation of the N-terminal group (see Table II). If the three-dimensional structure exists in a conformation that corresponds to that which appears necessary for binding D-Ala-D-Ala peptides, the proximal CNH, FNH, and BNH bonds that constitute the carboxylate binding site are pointing in the same direction (cf. 6a). In this conformation the N-terminal amino group of the antibiotic is much closer to the C6 hydrogen if the configuration of G1′ has the *S* stereochemistry,[40] and as a consequence, the initial interpretation of this observation led to an errroneous configurational assignment at the G1′ center.

To resolve this apparent anomaly, Harris[41] has suggested that if the conformation **6a** is changed by effecting a 180° rotation of the CNH amide bond such that the carbonyl points into the pocket (cf. **6b**), the N-terminal amino group of a structure having

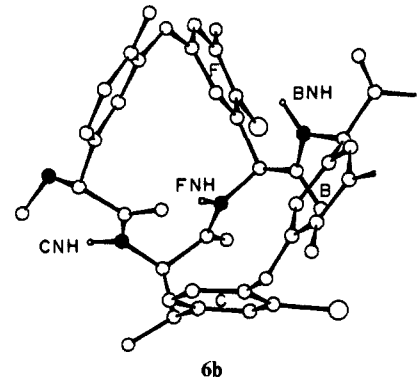

6b

the *R* configuration at G1′ would now be able to come closer to the C6 proton. While this suggestion is attractive, it is not consistent with the NOE results that we have obtained in the current study where a network of NOE's found in solvent B (in which the downfield shift of the C6 proton is observed) include G1′ ≫ CNH ≫ FNH ≫ BNH, which is clearly only consistent with the inside CNH conformation **6a**. At the moment, sufficient evidence is not available to provide an answer for this selective downfield shift of the C6 proton in acidic solvents.

Two additional conformational features that are relevant to defining the structure of the aglycon concern the sense of twist of the aromatic rings in both the biphenylactinoidinic acid subunit containing rings D and E and the biphenyl ether moiety that includes rings F and G.

The energy barrier for rotation about the bond linking the aromatic rings in actinoidinic acid is sufficiently high to allow isolation of the individual atropisomers.[22] Consequently, it would be expected that this bis(amino acid) fragment when in the more conformationally constrained environment of aridicin aglycon would be present in only one of the forms that differ in the sense of twist of the biphenyl chromophore. The biphenyl-type axial chirality of the actinoidinic acid segment in the aglycon is readily ascertained by reference to the disposition of the E6 and E2 hydrogens relative to the backbone hydrogens in the vicinity of the D and E rings. The NOE's observed for E2 to DNH and to A2′ in conjunction with the presence of cross peaks from E6 and ENH indicate that the plane of ring E is oriented in a manner that places the E2 hydrogen pointing into the interior of the binding pocket and the E6 hydrogen directed to the outer convex face as shown in partial structure 7.

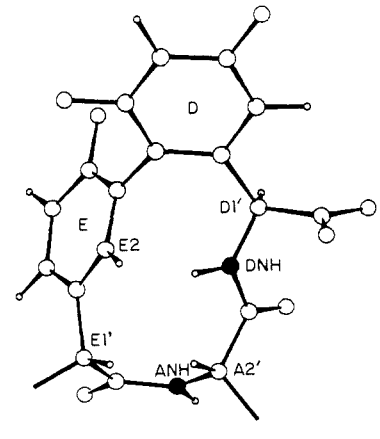

7

(39) Harris, C. M.; Harris, T. M. *J. Am. Chem. Soc.* **1982**, *104*, 4293–4295. Harris, C.; Kopecka, H.; Harris, T. M. *J. Am. Chem. Soc.* **1983**, *105*, 6915–6922.

(40) Williamson, M. P.; Williams, D. H. *J. Chem. Soc., Chem. Commun.* **1981**, 165–166.

(41) Harris, C. M.; Harris, T. M. *J. Am. Chem. Soc.* **1982**, *104*, 363–365.

Table VI. Comparison of Bond Angles Calculated from Vicinal ^1H Coupling Constants with Bond Angles for Conformer **6**

residue	^3J, Hz	θ(NH–CH), deg pred[42] from ^3J	θ(NH–CH), deg comp for **6**
A1′H–A2′H	0.8	85 or 95	−89
C1′H–C2′H	6.6	42 or 132	60
ANH–A2′H	11.9	167	−170
BNH–B1′H	8.0	25 or 139	−148
CNH–C2′H	8.2	23 or 141	163
DNH–D1′H	6.0	40 or 128	−126
ENH–E1′H	5.8	42 or 127	−124
FNH–F1′H	10.5	154	144
GNH–G1′H	not obsd		

All of the foregoing stereochemical and topological features were built into the model in the SK&F modeling system, and the structure was subjected to energy minimization using the MINIM program. The structure obtained by the refinement is represented in the computer-generated stereoprojection **6**. In the absence

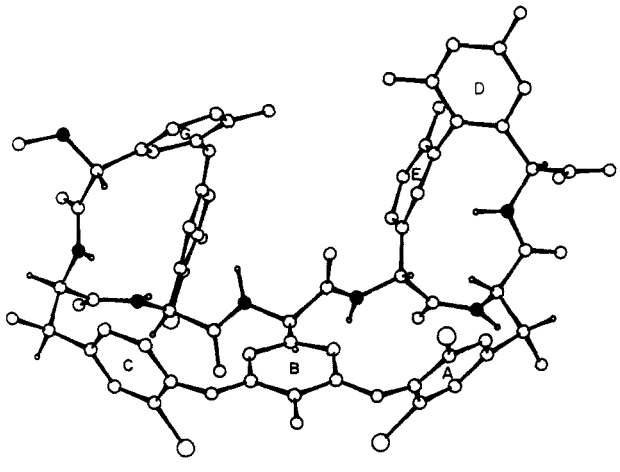

of an x-ray structure it is difficult to evaluate the accuracy of the structural coordinates derived for the proposed model. However, a comparison of the computed ^1H–^1H distances (Table IV), with a few exceptions, is in good agreement. The structure is also strongly supported by the close correlation of the predicted[42] NH–CH bond angles derived from ^1H coupling constants of aridicin aglycon with the values of the angles present in structure **6** (Table VI).[43]

The general details of the structure of the aglycon derived by the foregoing methods are in accord with the features established for other members of this family of antibiotics, which have been deduced by others.[23,29] However, in the majority of cases the previous results have relied on correlations with the X-ray structure of the vancomycin product CDP-I. The effort reported in this paper illustrates an alternative method requiring minimal chemical information and no correlations to other structures in this series in order to assign completely the three-dimensional structure of aridicin aglycon.

Structure of Aridicin A. With the structure of aridicin aglycon established, completion of the structure of aridicin A required locating the mannose and *N*-decanoyl-2-deoxy-2-aminoglucuronic acid residues and establishing the stereochemistry of their glycosidic linkages.

(42) Kopple, K.; Wiley, G. R.; Tauke, R. *Biopolymers* **1973**, *12*, 627–636.
(43) Evidence for the presence of other conformations in solution, principally those derived from **6** by small torsional librations about the CNH–G2′ carbonyl, is indicated. For example, the lower intensity of the volume integrals that are found for the NOE's between CNH, FNH, and BNH in comparison to the NOE's observed for hydrogens elsewhere in the molecule which are at comparable computed internuclear distances (A2′, E1′, DNH, and E2), suggests some motional flexibility in this local region of the molecule. Also, coupling constants for CNH in several solvents are found to vary over the range 6.5–8.2 Hz, which is indicative of the existence of different local conformational states in this region.

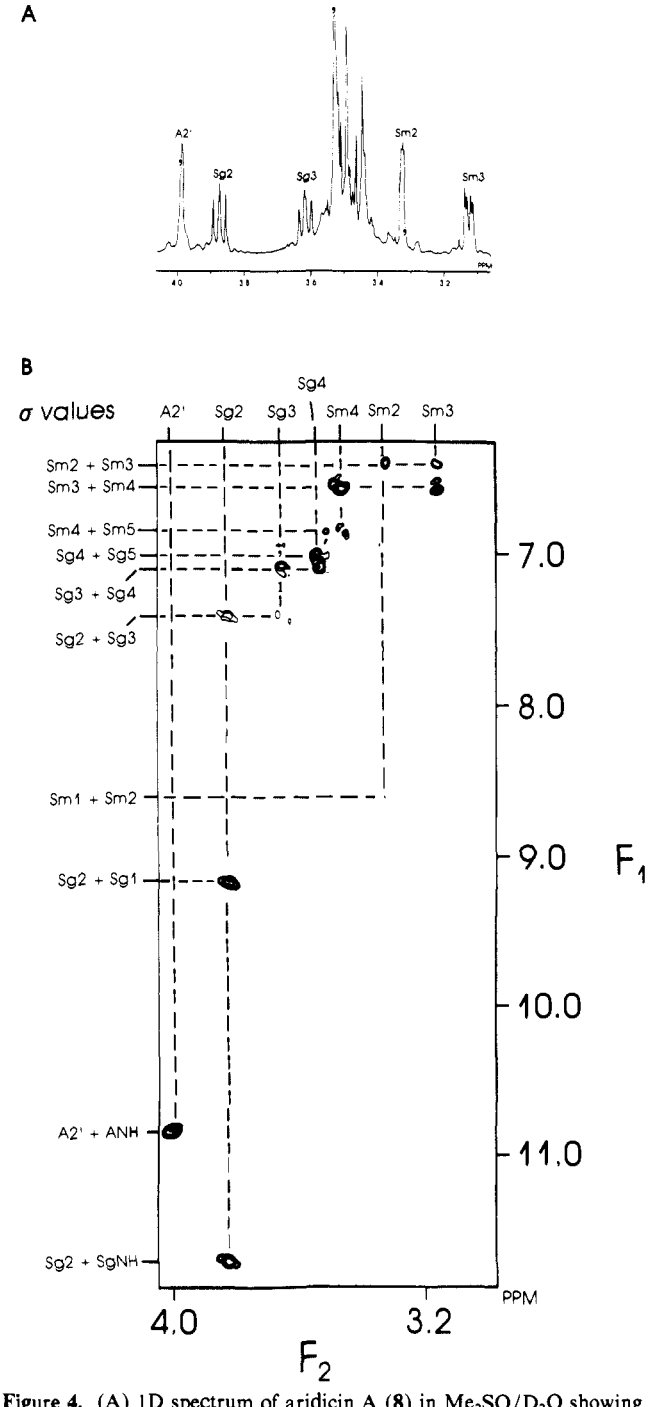

Figure 4. (A) 1D spectrum of aridicin A (**8**) in Me_2SO/D_2O showing complex sugar region and (B) double quantum spectrum of **8** in Me_2SO/H_2O (pH 5.6) showing sugar connectivities of both mannose (Sm) and 2-aminoglucuronic acid (Sg) residues. The latter spectrum was recorded at 40 °C by utilizing the pulse sequence as described in the Experimental Section with τ set to 17 ms. The spectral width was 8203.4 Mz in F_1 and 4201.7 Mz in F_2. A total of 512 t_1-fid's was recorded each of which contained 2K complex sampling points. Solvent peak suppression was accomplished by a combination of saturation by irradiation during the relaxation delay and during t_1 and by appropriate phase cycling. Sine bell functions in both frequency domains were applied before Fourier transformation.

Despite the more demanding restrictions previously encountered in obtaining well-resolved ^1H spectra of intact antibiotics in this series, highly resolved spectra with line widths of <1.0 Hz were obtained for aridicin A, its pseudoaglycon, and the mannosyl aglycon in D_2O (H_2O)/Me_2SO-d_6 (1:1, v/v) solvent mixtures at a pH 5.6–7.6 (see Figure 4A). With this resolution it was possible to undertake delayed COSY experiments to establish connectivities through long-range J couplings. Also, the availability of high-

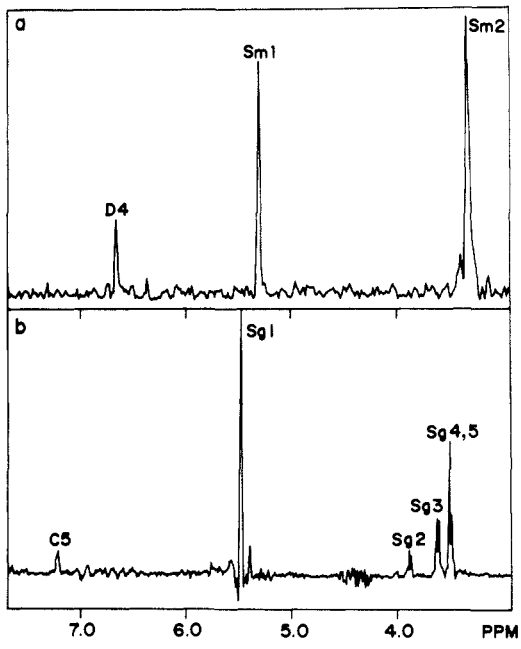

Figure 5. (a) Cross section through Sm1 axis of delayed COSY spectrum of aridicin A showing long-range coupling between Sm1 and D4. Fixed delays of 300 ms before and 60 ms after the mixing pulse were inserted. The sample was dissolved in Me_2SO-d_6/D_2O mixture. (b) Cross section through Sg1 showing NOE cross peak between proton signals at Sg1 and C5 in the NOESY spectrum of aridicin A.

resolution ID ^1H spectra of aridicin A and its hydrolysis products, aridicin aglycon, pseudoaglycon, and the mannosyl aglycon, allowed comparisons to be made that facilitated the assignments of individual proton chemical shifts of the mannose (Sm) and glycolipid (Sg) residues, many of which overlap in the 500-Mz spectrum of aridicin A (the utility of a double quantum experiment that diminishes the need for such comparisons is discussed subsequently).

Position of the Carbohydrate Residues. The location of the mannose residues at position 5 in ring D was indicated by several independent spectroscopic methods. Chemical shifts arguments for positioning mannose at D5 in the related antibiotic teichoplanin have been previously advanced by Hunt and co-workers.[23] Consistent with these results, the aromatic proton signals assigned to D2 and D4 were shifted upfield 0.20 and 0.35 ppm, respectively, in the 500-MHz spectrum of the aglycon relative to the corresponding signals in the spectra of aridicin A and the mannosyl aglycon. The interpretation of this result depends on the unambiguous assignment of the D2 and D4 hydrogen signals. The presence of weak cross peaks between D1′ and D2 in both the delayed COSY and the NOESY spectra of aridicin A confirmed the assignment of the D2 resonance. For this reason we are confident that the D2 and D4 hydrogen signals in the spectrum of **2** (solvent A) are assigned correctly as δ 6.33 and 6.39, respectively, and the location of the mannose residue at the 5-position of ring D is supported. Also in accord with this assignment are the NOESY spectra of aridicin A and mannosyl aglycon, each of which shows a cross peak between the D4 signal and a proton signal at δ 5.30 attributable to the C1 anomeric hydrogen (Sm1) in the mannose ring. However, the most definitive evidence for placing the mannose residue was obtained from the delayed COSY ^1H spectra of aridicin A and mannosyl aglycon, which show long-range coupling through the glycosidic oxygen between hydrogens at Sm1 (5.30) and D4 (δ 6.67) convincingly pinpoint the location of the mannose at D5 (see Figure 5a).

The location of the site of attachment of the 2-deoxy-2[(1-oxodecyl)amino]-D-glucopyranosiduronic acid residue proved more difficult. There were no significant chemical shift displacements found when comparing the ^1H spectra of **2**, aridicin A, pseudoaglycon, and mannosyl aglycon other than those associated with D2 and D4 discussed previously. Furthermore, the anomeric hydrogen signal of the amino sugar residue in aridicin A and the pseudoaglycon, which occurs at δ 5.47 and 5.51, respectively, in these compounds shows no observable cross peaks in the delayed COSY experiment. While there are six possible sites for attachment of this residue, the A1′ and C1′ hydroxyl groups and the four phenol oxygen sites at B4, E4, F3, and G4, only its attachment at B4 is consistent with these results. Fortunately, this conclusion was supported by positive experimental results; the NOESY spectra of aridicin A and the pseudoaglycon both show evidence for a through-space interaction between the anomeric proton (Sg1) and the C5 proton in the peptide. This is clearly revealed in Figure 5b, which shows a weak cross peak to C5 in the Sg1 cross section of the 2D NOE spectrum of aridicin A. Despite the fact that this cross peak is relatively weak, its presence in the spectra of both aridicin A and the pseudoaglycon, coupled with the clear absence of a cross peak at this location in the NOESY spectra of **2** and the mannosyl aglycon, constitutes good evidence for the interaction. Inspection of a CPK model (which tends to overemphasize conformational rigidity) indicates that the pendant amino sugar residue at B4 has some local motional flexibility at the glycosidic linkage that would reduce the intensity of the cross peak resulting from the through-space interaction between the Sg1 and C5 protons.

Stereochemistry of Glycosidic Links and Ring Size of the Sugars. The structural issues remaining that relate to each of the carbohydrate components concern the ring size and the stereochemistry of the glycosidic links to the heptapeptide core. Resolution of these points was readily accomplished from consideration of the ^1H–^1H coupling constant data for each of the carbohydrate rings initially on the pseudoaglycon and the mannosyl aglycon and subsequently in the intact antibiotic for confirmation.

The anomeric proton signal of Sg1 in the ^1H spectrum of the pseudoaglycon appeared as a doublet with a 8.5-Hz coupling to Sg2, which was clearly indicative of the aminouronic acid residue attached to B4 through a β-anomeric linkage. Assignment of the 2-deoxy-2-[(1-oxodecyl)amino]-β-D-glucopyranosiduronic acid structure was supported by the large values of the ^3J coupling constants, which ranged from 8.5 to 10.0 Hz, typical of trans-diaxial coupling for β-D-glucopyranoside in a $^4C_1$ conformation,[44,45] and was corroborated by the appearance of strong cross peaks in the NOESY spectrum of the pseudoaglycon between the syn-axial protons (Sg1, Sg3, Sg5 and Sg2, Sg4).

Similar arguments led to the characterization of the mannosyl aglycon as containing the carbohydrate as the α-D-mannopyranoside. The value of $J_{1,2}$ = 1.5 Hz is indicative of the α-anomeric linkage.[44] Confirmation of this was found in the 2D NOE data where strong through-space coupling was observed between Sm1 and Sm2. No NOE cross-peak was found between Sm1 and Sm3, as should occur in the β-anomer. Again the $J_{3,4}$ coupling of 8–9 Hz is sufficient to establish the existence of the mannose in the $^4C_1$ pyranoside form.[44,45]

From the foregoing evidence we conclude that the structures of aridicin A, the pseudoaglycon, and the mannosyl aglycon are as depicted in structures **8**–**10**, respectively.

While the availability of both **9** and **10** simplified the task of assigning the ring protons in both carbohydrates, the difficulty of effecting the selective removal of carbohydrates located at various sites in most antibiotics of this class may frequently preclude such an approach. Consequently, the desirability of having a general method to solve the assignment problem that is created by overlapping resonances from two or more carbohydrate moieties in these glycopeptide antibiotics was apparent.

A double quantum experiment on aridicin A in H_2O/Me_2SO proved especially useful in interpreting these regions of the

(44) Hall, L. D. In *The Carbohydrates 1980*; Pigman, E., Hortan, D., Eds.; Academic: New York, 1980; Vol. 1B, p 1299. Coxen, B. *Adv. Carbohydr. Chem. Biochem.* **1972**, *27*, 7–83.

(45) Angyal, S. *Carbohydr. Res.* **1979**, *77*, 37–50. Coxon, B. *Carbohydr. Res.* **1968**, *8*, 125–134. Haasnoot, C. A. G.; DeLeeuw, F. A. A. M.; Altona, C. *Org. Magn. Reson.* **1981**, *15*, 43–52.

(46) Wagner, G.; Zuiderweg, E. R. P. *Biochem. Biophys. Res. Commun.* **1983**, *113*, 854–860. Macura, S.; Kumar, N. G.; Brown, L. R. *Ibid.* **1983**, *117*, 486–492.

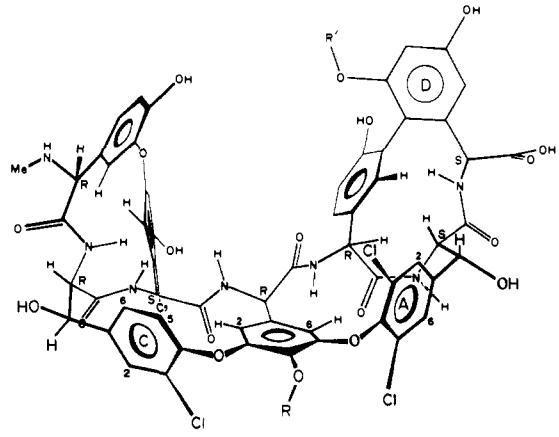

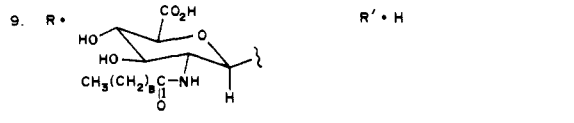

spectrum containing strongly coupled, overlapping resonances of the sugar ring protons (see Figure 4A). Also, the latter occur in the same region as the strong H_2O signal from the solvent, which is largely suppressed under the conditions of the double quantum excitation.[47] The resulting spectrum obtained at pH 5.6 contained seven amide NH signals that could be identified and assigned from double quantum cross peaks to neighboring α-CH protons. Most interestingly, a clear coupling pattern was evident for each of the protons in the two sugar rings in the contour plot of the 2D double quantum spectrum of **8**, a segment of which is shown in Figure 4B.

In double quantum transitions, pairs of spins i and j resonate at the sum of their corresponding chemical shift frequencies $\sigma_i + \sigma_j$. These transitions are indirectly observed via the allowed single quantum transitions of both participating nuclear spins. Hence, in double quantum spectra, pairs of peaks appear in F_1, which are centered around the axis $(2F_1,F_2)$, with coordinates of $\sigma_i + \sigma_j$ in F_1 and σ_i and σ_j in F_2.

In the upper part of the depicted portion of the double quantum spectrum, these pairs of peaks are clearly visible for the double quantum transitions of (Sm2, Sm3), (Sm3, Sm4), and (Sg3, Sg4). In other cases, particularly in the lower part of the figure, only one of the observed double quantum peaks is visible, and the complementary peaks appear at chemical shift positions in F_2 outside the displayed range, e.g., σ_{SgNH} is at 7.83 ppm.

Conclusion

The structures of aridicin A and its aglycon are derived as **8** and **2**, respectively, from studies based upon a variety of two-dimensional NMR methods. The NMR results, particularly those obtained from 2D NOE spectra, provide approximate intramolecular hydrogen distances that, when used as distance constraints, provide the expeerimental data for interactive computer-assisted modeling to derive the three-dimensional structure of the aglycon **2**. Elaboration of the remaining details of the parent antibiotic is accomplished by further NMR studies in which delayed COSY, NOESY, and double quantum methods are employed.

The methods described here not only should prove especially useful in providing detailed structural information on new members of this class of molecules but also should be readily applicable to other classes of complex structures.

Acknowledgment. We are indebted to Dr. D. Hare for providing an advanced copy of his NMR program and to Dr. J. Hempel for useful discussions. Dr. Robert Sitrin and his associates, G. Chan and G. Udowenko, are thanked for providing the samples used in this study.

Registry No. 2, 101630-74-4; **8**, 95935-21-0.

(47) Macura, S.; Kumar, N. G.; Brown, L. R. *J. Magn. Reson.* **1984**, *60*, 99-105.

Stereochemistry and Total Synthesis of Amavadin, the Naturally Occurring Vanadium Compound of *Amanita muscaria*

H. Kneifel[†] and E. Bayer*[‡]

Contribution from the Institute of Organic Chemistry, University of Tuebingen, D-7400 Tuebingen, West Germany, and Institute for Biotechnology, KFA, D-5170 Juelich, West Germany. *Received October 15, 1985*

Abstract: The structure and stereochemistry of the vanadium compound of *Amanita muscaria*, amavadin, are elucidated, and a total synthesis of amavadin is reported. It is shown to be the monohydrated complex of VO^{2+} with two molecules of *N*-(L-1-carboxyethyl)-*N*-hydroxy-L-alanine. The ligand belongs to a new type of complexing agents. Amavadin is the first naturally occurring vanadium compound of which the structure of an organic ligand has been established and synthesized.

Vanadium recently has attracted increasing interest in biochemistry.[1,2] Of the numerous effects of vanadium on organisms reported, its stimulatory effect on the growth of algae and plants[3] and the inhibitory action of vanadate(V) on Na,K-ATPase[4] are especially worth mentioning. However, there is still little knowledge about the structure and biological function of naturally

[†] Institute for Biotechnology, KFA.
[‡] University of Tuebingen.

(1) Schwarz, K.; Milne, D. B. *Science (Washington, D.C.)* **1971**, *174*, 426.
(2) See recent reviews: Chasteen, N. D. *Struct. Bonding (Berlin)* **1983**, *53*, 105. Kustin, K.; Macara, I. *Comments Inorg. Chem.* **1982**, *2*, 1.
(3) Meisch, H.-U.; Bielig, H.-J. *Basic Res. Cardiol.* **1980**, *75*, 413.

0002-7863/86/1508-3075$01.50/0